Elucidation of the Electronic Structure of Molecules with the Help of NMR Spin−Spin Coupling Constants: The FH Molecule

Jürgen Gräfenstein, Tell Tuttle, and Dieter Cremer*

Department of Theoretical Chemistry, Göteborg University, Reutersgatan 2, S-41320 Göteborg, Sweden

Received: October 5, 2004; In Final Form: December 3, 2004

It is demonstrated how the one-bond NMR spin−spin coupling constant (SSCC) ^1J(FH) can be used as a source of information on the electronic structure of the FH molecule. For this purpose, the best possible agreement between measured and calculated SSCC is achieved by large basis set coupled perturbed density functional theory calculations. Then, the calculated value is dissected into its four Ramsey terms: Fermi contact, the paramagnetic spin−orbit term, the diamagnetic spin−orbit term, and the spin dipole term, which in turn are decomposed into orbital contributions and then described by their spin densities and orbital current densities. In this way, the SSCC gives detailed information about the electronegativity of F, the bond polarity, the bond polarizability, the volume and the polarizability of σ and π lone pair orbitals, the s- or p-character of the bond orbital, the nature of the LUMO, and the density distribution around F.

1. Introduction

The indirect spin−spin coupling constants (SSCCs) J of nuclear magnetic resonance (NMR) spectroscopy is a sensitive antenna for detecting features of the electronic structure, the geometry, and conformation of a molecule.[1] Spin−spin coupling information is transferred between the coupling nuclei both through the network of bonds and through-space. By the sign and the magnitude of the measured or calculated SSCCs, one obtains insight into the electron density distribution and the structural features of the molecule. Ramsey[2] distinguished between a spin polarization and an orbital current mechanism both invoked by the magnetic moments of the coupling nuclei. At the contact surface of a nucleus the spin density is directly polarized by Fermi coupling and this spin polarization travels through the molecule like a wave thus yielding the Fermi contact (FC) contribution to the SSCC. Similarly, the dipole field of the nuclear moment causes spin polarization, which is sensed by the quadrupolar potential of the other nuclei and thus leads to the spin dipole (SD) contribution of the SSCC. The orbital currents induced by the magnetic moments can be split (somewhat arbitrarily but nevertheless useful) into a diamagnetic spin−orbit (DSO) and paramagnetic spin−orbit (PSO) contribution. All four terms together establish the Ramsey mechanism[2] of indirect (i.e., mediated through the electron density) spin−spin coupling.[3−10]

The transmission of spin−spin coupling information from the perturbing to the responding nucleus depends as indicated by the Ramsey mechanism strongly on the electronic structure of a given molecule and in this way also on its geometry and conformation. There are numerous review articles that describe the dependence of the SSCC on geometrical and conformational parameters[1,11−13] of which the work on the Karplus relationship is best known.[14−16] There is also extensive work on the relationship between charge distribution, orbital hybridization, and contact densities to explain the FC term.[11−21] These approaches proved successful in reproducing qualitatively many trends observed for SSCCs. Noteworthy in this connection are investigations carried out by Contreras and co-workers[11−13] who carefully studied the transmission mechanism of many different SSCCs and who provided simple explanations for observed SSCCs.

The development of reliable methods to calculate SSCCs in a routine manner[5−10] has provided for the first time a platform to systematically analyze the spin−spin coupling mechanism. We have recently developed the J-OC-OC-PSP = J-**OC**-PSP method (decomposition of J into orbital contributions using orbital currents and partial spin polarization)),[22,23] which makes it possible to dissect the calculated indirect isotropic SSCC into orbital terms and to interpret these terms with the help of Ramsey densities, orbital current densities, and graphical representations of zeroth- and first-order orbitals. In a number of publications, we have demonstrated the usefulness of J-**OC**-PSP when analyzing one-bond SSCCs,[22] spin−spin coupling via π-bonds[23] or across H-bonds in proteins,[24,25] the SD coupling mechanism in comparison with the FC mechanism,[26] the role of the DSO and the PSO coupling mechanism,[27] the analysis of multipath coupling,[28,29] the description of multiple bonds with the help of the noncontact terms SD, DSO, and PSO,[30] the quantification of π-delocalization across formal single bonds with the help of the PSO term,[31] or long-range coupling in polyenes.[32] A critical comparison of the J-**OC**-PSP method with other methods and a systematization of analysis strategies was also presented.[33]

Recently, we have identified the basic one- and two-electron effects that are responsible for the spin−spin coupling process.[34] They involve Ramsey response, first-order delocalization, and steric exchange effects. Although the electronic theory of the basic spin−spin coupling mechanism was formulated for all four Ramsey terms, it was applied for the relative simple coupling mechanisms of ^{13}C−^{1}H and ^{1}H−^{1}H coupling in methane, which is dominated by FC coupling. In this work, we will apply the analysis to SSCC for which all four Ramsey terms play a role, namely for the transfer of spin information between the nuclei ^{19}F and ^{1}H of the FH molecule. The analysis will show that even for the apparently simple case of a diatomic molecule a

10.1021/jp045463w CCC: $30.25
Published on Web 02/22/2005

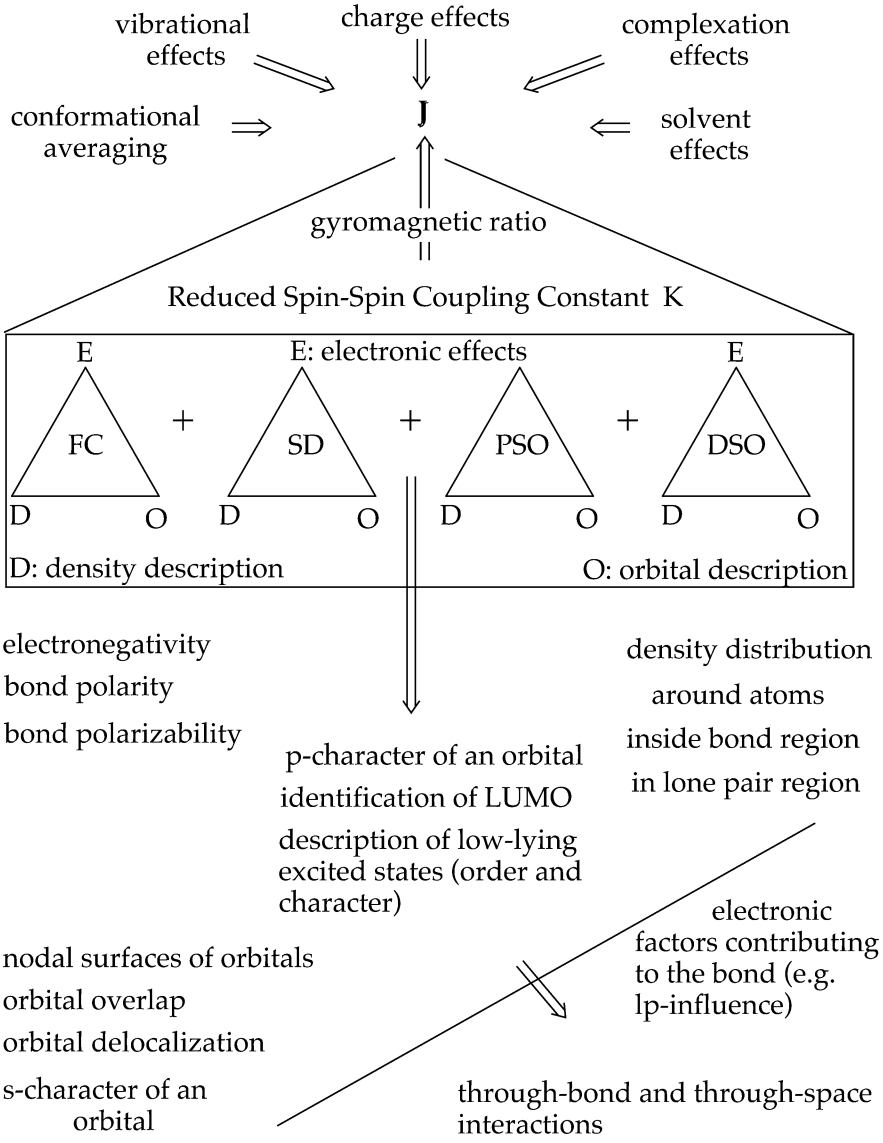

Figure 1. NMR spin−spin coupling constant arises from the four Ramsey terms FC, SD, PSO, and DSO. Each of these terms can be described with the help of orbital contributions *O* and density distributions *D* to identify the electronic effects E responsible for the coupling mechanism. Effects that influence measured *J* values are also shown.

wide range of different effects contributes to the total spin−spin coupling and that important conclusions can be drawn for spin−spin coupling in general. Especially, we will show that theory can be used to extract from a single measured SSCC direct information on the electronic structure of a molecule, which otherwise would only be available by a series of spectroscopic measurements.

2. A Systematic Way of Analyzing the NMR Spin−Spin Coupling Constants

For the purpose of analyzing the electronic effects responsible for spin−spin coupling, one has to separate those influences that may disguise the actual electronic effects. The measured SSCC corresponds to the isotropic average of the spin−spin coupling tensor. Both the tensor and the isotropic average can be calculated and directly be compared with what is experimentally available. The experimentally measured SSCC is affected not only by the electronic coupling mechanism between the nuclei but also by their gyromagnetic ratios. Thus, the calculated reduced SSCC *K*, which depends just on the electron density mediating the coupling mechanism, has to be converted into the measured SSCC *J* according to eq 1

$$J_{A,B} = \left(\frac{h \cdot \gamma_A \cdot \gamma_B}{4\pi^2}\right) K_{A,B} \qquad (1)$$

where γ_A and γ_B are the gyromagnetic ratios of the coupling nuclei *A* and *B*, respectively. Measured SSCCs comprise vibrational effects and environmental effects (Figure 1). The former have been determined for a number of small molecules;[35] however there is presently no analytical method available that leads to a routine calculation of vibrational effects for *J*. Generally one can say that vibrational effects are significant for SSCCs involving protons whereas they are small for spin−spin coupling between heavy atoms. More serious are differences between measured and calculated SSCCs in the case of large amplitude vibrations such as internal rotations, ring inversion or ring pseudorotation. In these cases, the dependence of the SSCC on conformational parameters can be calculated and an average value obtained using Boltzmann statistics.[36,37]

Specific (complexation by solvent molecules) and nonspecific solvation effects have to be considered when comparing

TABLE 1: Basic Electronic Effects Acting in the NMR Spin−Spin Coupling Mechanism of a Diatomic Molecule[a]

term	orbitals[b] space LMOs	electrons[c]	calculation	method	important for FC	SD	PSO
Ramsey distortion	one active l	one+two	self-consistent	CP	×	×	×
direct Ramsey response		one	direct	SOS	×	×	×
self-exchange interaction		two	self-consistent	CP − SOS	×	×	(×)
echo effect	active l + passive l′	one+two	self-consistent	CP	×	×	
first-order delocalization		one	direct	SOS	×	×	
steric exchange		two	self-consistent	CP − SOS	×	×	
external orbital contribution	active l + active l′	one+two	self-consistent	CP	×	×	(×)
first-order delocalization		one	direct	SOS	×	×	
steric exchange		two	self-consistent	CP − SOS	×	×	(×)
two-orbital spin transport	active k + active l	two	self-consistent	CP − SOS	not possible for ^1J		
first-order delocalization		one	direct	SOS			
steric exchange		two	self-consistent	CP − SOS			
three-, four-, ... orbital spin transport	active k, l + passive m, ...	two	self-consistent	CP − SOS	not possible for ^1J		
first-order delocalization		one	direct	SOS			
steric exchange		two	self-consistent	CP − SOS			

[a] The DSO mechanism is a zeroth-order effect and does not involve any changes of the orbitals. [b] k, l, m, ..., are orbitals in the bond path; l′ is an orbital outside the bond path. [c] Here, "one" denotes one-particle effects (connected with kinetic and electron−nuclear attraction energy), "two" stands for electron−electron repulsion effects.

experimental and calculated SSCCs.[38,39] Often these influences can be neglected when the measurement is carried out in a nonpolar solvent without any specific solvation effects. In the case of specific solvation, it is desirable to investigate the complexes formed directly so that these effects are already included into the zeroth-order description. The same will be advisable if effects of cations or anions are encountered as in the case of biochemical molecules in aqueous solution.[24,25]

Once it is clarified that calculated and measured SSCCs are comparable, their signs and magnitudes can be analyzed by first dissecting the total SSCC into their Ramsey terms (Figure 1) and then describing each Ramsey term in form of orbital and spin density contributions to determine the electronic effects that play the most important role for a given spin−spin coupling mechanism.

The spin information can be transferred between the two coupling nuclei along different kinds of orbital paths. In the simplest case, which we call *Ramsey distortion*,[23,34] an orbital is distorted by the perturbing nucleus and this distortion directly causes a magnetic field at the responding nucleus. This effect can be estimated from the first-order orbital or the appropriate spin or orbital current density. The form of the operator leads to certain selection rules,[26,27] which help to identify those orbitals with large (small) Ramsey contributions. For example, σ-orbitals with a large s-contribution at both coupling nuclei play a dominant role for the FC term whereas orbitals with a large p-contribution at both coupling nuclei are essential for sizable SD and PSO terms.[26,27]

The Ramsey distortion takes place in two steps: In the initial *direct Ramsey response* (Table 1), the orbitals react directly to the external perturbation. Consequently, the charge centroids of α and β electrons in the orbital concerned are shifted against each other, and the two electrons exert a repelling force on each other. In the second step, this repelling force enhances the mutual shift of the two charge centroids and influences (usually increases) thus the Ramsey distortion and eventually its contribution to the SSCC. This second step decreases the $\alpha-\beta$ repulsion energy in the orbital. The total electron density, and thus the total Hartree interaction of the two electrons (self-interaction plus $\alpha-\beta$ repulsion energy), remains unchanged in first order for magnetic perturbations. Therefore, the minimization of the $\alpha-\beta$ repulsion energy formally appears as a maximization of the self-exchange energy in the coupled perturbed (CP)-DFT equations, and the second step of the Ramsey distortion is therefore called *self-exchange interaction* (Table 1). The direct Ramsey response is a *one-orbital one-electron process*; i.e., the two electrons in the space orbital respond to the perturbation individually, and the self-exchange interaction is a *one-orbital two-electron process* reflecting the interaction of the two electrons in the bond.

The discussion above is related to the FC and SD terms, where the perturbing nucleus gives rise to spin polarization of the electron system. For the PSO term, the perturbation generates an orbital current that is equal for α and β obitals. The orbital current will also influence the exchange interaction and thus will lead to similar two-electron effects as for the FC and SD terms.

For one-bond SSCCs, Ramsey distortions usually make the dominating contributions to the total spin−spin coupling. However, even in this apparently simple case, the spin information may be transferred through the system on paths involving more than one orbital. One important process proceeds in the way that the bond orbital polarizes one of the surrounding orbitals, which gives a feedback on the bond orbital and thus influences the spin−spin coupling. If such an *echo effect* (Table 1)[23,34] occurs, only the bond orbital will act as an *active orbital*, i.e., will exchange spin information with the nuclei. The second intervening orbital acts *passively*, i.e., influences the spin−spin coupling without direct interaction with any of the coupling nuclei.

Another important two-orbital process proceeds in the way that one of the coupling nuclei interacts with another orbital outside the bond path rather than with the bond orbital. The *external orbital* in turn passes the spin information to the bond orbital. For these *external orbital contributions* (Table 1), both orbitals involved act actively.

For geminal, vicinal, etc. SSCCs the bond path between the coupling nuclei consists of several bonds. In this case, *spin transport* processes (Table 1) become increasingly important, where the spin information is passed from bond to bond along the bond path, i.e., *through-bond*. If two orbitals are involved in the spin transport, both of them are active. For three or more orbitals, in contrast, one or more orbitals act passively.[23] Usually, through-bond spin transport through three or more orbitals will be efficient only in unsaturated molecules if the intermediate passive orbitals are part of the π system.[23,31−33] Sizable vicinal or higher-order SSCCs in, e.g., alkanes are usually due to

through-space coupling, where one or more orbitals in the bond path are skipped in the spin-information transport.

For all coupling mechanisms that involve two or more orbitals, there are two different mechanisms to transfer the spin information from one orbital to the next in analogy to the two mechanisms occurring for the Ramsey distortion. The most obvious one is the *steric exchange interaction* (Table 1)[23,34] where the spin polarization in one orbital causes spin polarizations in the surrounding orbitals in a way that the opposite-spin overlap, and thus the electrostatic repulsion energy, in the electron system is minimized. Formally, this procedure is described as a maximization of the exchange energy between different equal-spin electrons, which accounts for the denotation "steric exchange interaction". A detailed analysis[34] shows that there is in addition a *first-order delocalization interaction* between the orbitals (Table 1), which is independent of the electron−electron interaction: If one orbital is deformed by the perturbing magnetic moment, then all other orbitals will readjust to minimize the total one-particle energy under the constraints given by the Pauli principle. The first-order delocalization effect can thus be classified as a *two-orbital one-electron process*, in the sense that it concerns the one-particle properties of the electrons involved, i.e., kinetic and electron-nucleus attraction energy, whereas the steric repulsion energy is a *two-orbital two-electron process*, concerning the $\alpha-\beta$ repulsion energy of electrons in different orbitals.

The J-**OC**-PSP method[22,23,34] allows one to decompose the total SSCC as well as its Ramsey terms into orbital contributions. At the J-**OC**-PSP1 level,[22,23] the decomposition is based on the active contributions of the orbitals involved, which leads to a decomposition into one- and two-orbital contributions. At this level of theory, passive orbital contributions such as echo effects cannot be determined. This requires the J-**OC**-PSP2 level,[23] where both active and passive orbital contributions can be investigated, leading to one-, two-, three-, ..., *n*-orbital terms.

Recently, we demonstrated how the J-**OC**-PSP contributions can be decomposed into one-electron and two-electron contributions.[34] For this purpose, the analysis is repeated with sum-over-states density functional perturbation theory (SOS-DFPT)[9,34] where the two-electron effects in the response to the perturbing nuclear moment are suppressed. This step provides the direct Ramsey response and first-order delocalization parts of the J-**OC**-PSP contributions. The difference between the CP-DFT and SOS-DFPT values of each J-OC-PSP contribution determines self-exchange or steric-exchange interaction, respectively.

One might argue that repeated calculations of the different terms of one SSCC, which is required in the J-**OC**-PSP analysis, become too expensive. However, the calculation of SSCCs at the CP-DFT level is not expensive and can be repeated several times without dramatic cost increases. In addition, experience shows that for larger molecules (i) only single SSCCs are interesting enough to be analyzed in detail and (ii) only a limited set of orbital paths are relevant to understand the mechanism behind these SSCCs. The J-**OC**-PSP analysis can thus be applied in these cases in a few steps by systematically changing selected groups of orbitals (rather than single orbitals) from frozen to passive, and then to active.

A complementary tool, which can be used to describe electronic effects identified with the help of orbital contributions, is provided by the graphical representation of spin polarization density and orbital current density distributions that carry the spin information from the perturbing to the responding nucleus.[22,23,26,27,31] In this way, the Ramsey terms and their orbital contributions are related to local quantities, which is an important analytical tool within the J-OC-PSP approach.[22,23] For the FC term this is the *FC spin density distribution* $m^{(B),FC}(\mathbf{r})$, i.e., the spin density generated in the electron system by the FC perturbation of nucleus B,[22]

The representation of the noncontact Ramsey terms becomes more complex because these terms (a) are anisotropic and (b) the corresponding perturbation operators are not localized at the responding nucleus. For each of the noncontact terms, we introduced therefore two kinds of local densities, which reflect the two-step mechanism of spin−spin coupling:[26,27]

(a) The first is a *spin (SD) or current (PSO, DSO) density*, reflecting the interaction of the perturbed nucleus with the electron system. These densities are vector quantities and depend on the orientation of the perturbed spin. The spin or current densities are specific for the perturbed but independent of the responding nucleus. The DSO and PSO current densities for the perturbing nucleus spin-oriented along *i* are $\mathbf{j}_i^{(B),DSO}(\mathbf{r})$ and $\mathbf{j}_i^{(B),PSO}(\mathbf{r})$.

The calculation and investigation of the SD term can be simplified if the SD spin density is decomposed into subcomponents according to $\mathbf{m}_i^{(B),SD}(\mathbf{r}) = \sum_j{}' m_{(ij)}^{(B),SD}(\mathbf{r})\mathbf{n}_j$ where index *i* gives the orientation of the perturbing nuclear spin and index *j* ($i, j = x, y, z$) denotes the component of the SD-spin density distribution $\mathbf{m}_i^{(B),SD}$ under consideration, with $\mathbf{n}_j$ being the normal vector in direction *j*. Hence, there are the six subcomponents (*xx*), (*xy*), (*xz*), (*yy*), (*yz*), and (*zz*) for the SD spin density. These subcomponents must not be confused with the diagonal and nondiagonal components of the spin−spin coupling tensor. The indices for the subcomponents will be enclosed in parentheses to mark the difference.

(b) Seond is an *energy density*, which is the spin or current density weighted with the perturbation operator at the responding nucleus. This density, which is scalar for all three noncontact terms, can be averaged over all orientations of the perturbing nuclear spin, which provides the energy densities for the isotropic Ramsey terms. The energy densities depend on both the perturbing and the responding nucleus and the orientation of their magnetic moments. For the isotropic average of the SSCC, only the diagonal components of the energy density are of interest, where the two magnetic moments are oriented parallel. These are the Ramsey energy densities $\rho_{ii}^{(AB),DSO}(\mathbf{r})$ and $\rho_{ii}^{(AB),PSO}(\mathbf{r})$. The diagonal components of the SD energy density and the isotropic SD energy density distribution are $\rho_{ii}^{(AB),SD}(\mathbf{r}) = \sum_i \rho_{(ii')}^{(AB),SD}(\mathbf{r})$ and $\rho^{(AB),SD}(\mathbf{r}) = {}^1/_3\sum_i \rho_{ii}^{(AB),SD}(\mathbf{r})$. Details on how to calculate these quantities are given elsewhere.[22,23,26,27]

Scheme 1 provides an overview over the spin, current, and energy densities as well as their components and subcomponents for the example of the *zz* component of the SSCC.

In the following, we will unravel the information contained in one SSCC when this is partitioned into Ramsey terms, which in turn are decomposed into orbital contributions. For this purpose we have chosen the one-bond SSCC $^1J(^{19}F^1H) = {}^1J(FH)$ of hydrogen fluoride, which provides an example for a nontrivial, interesting spin−spin coupling mechanism.

3. Computational Details

All SSCC calculations described in this work were carried out with the CP-DFT method of Sychrovský, Gräfenstein, and Cremer.[9] Utilizing the experience of these authors, who systematically studied the influence of DFT and exact exchange on the value of the SSCC, and the fact that standard procedures lead to poor values for $^1J(^{19}F^1H) = {}^1J(FH)$,[9,40] we employed a

SCHEME 1: Overview over the Spin, Current, and Energy Densities as Well as Their Components and Subcomponents, Exemplified for the *zz* Component of the SSCC Tensor[a]

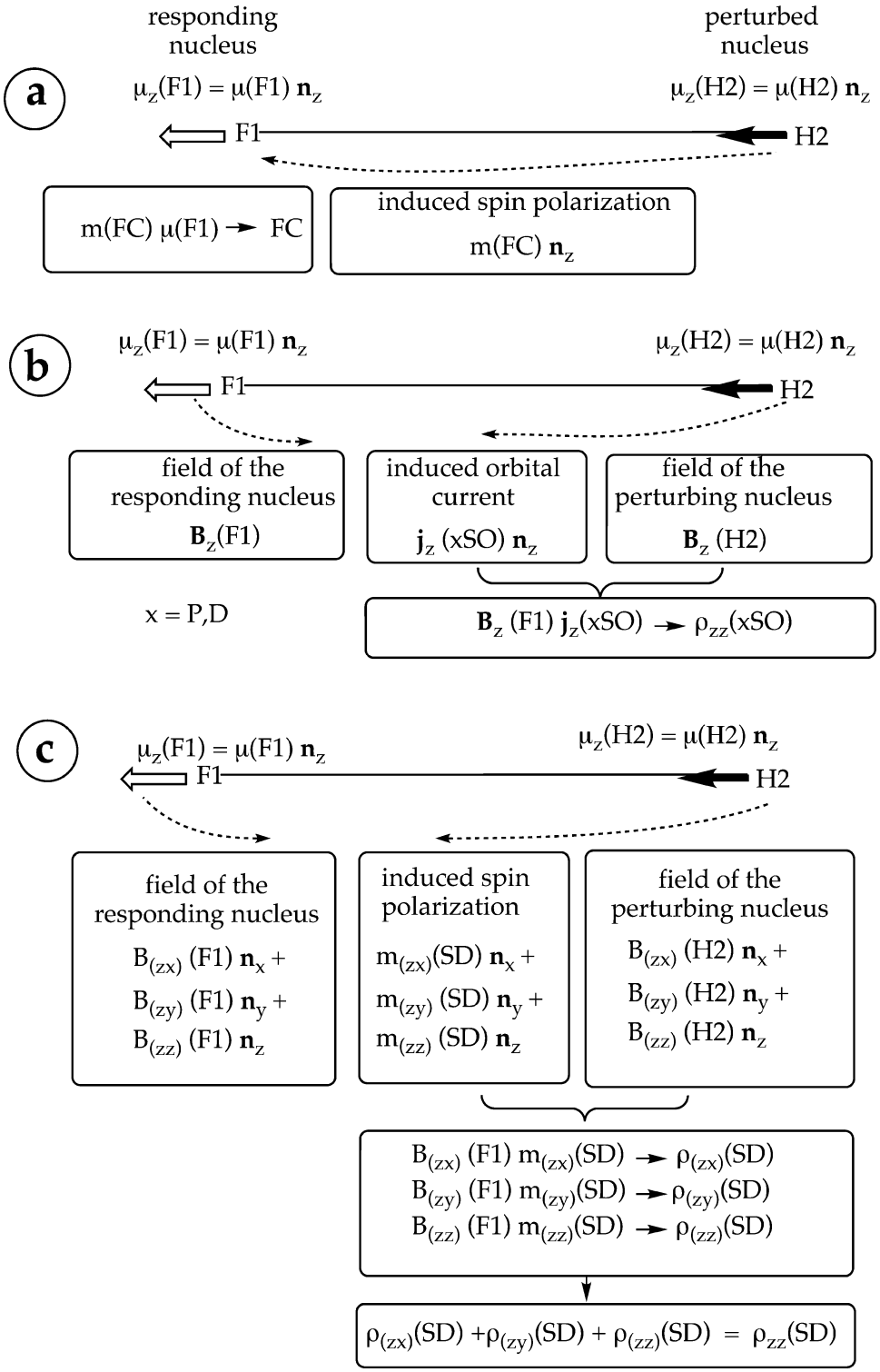

[a] Key: (a) For the FC term, the magnetic moment $\vec{\mu}_z$(H2) = μ(H2)$\mathbf{n}_z$ of the perturbed nucleus ($\mathbf{n}_z$ is the *z* unit vector) generates a spin polarization *m*(FC) that is parallel to $\mathbf{n}_z$. The moment $\vec{\mu}_z$(F1) of the responding nucleus senses this spin polarization locally. (b) For the PSO and DSO terms, $\vec{\mu}_z$(H2) generates the magnetic field $\mathbf{B}_z$(H2), which in turn generates the orbital current $\mathbf{j}_z$(*x*SO) (*x* = P,D). The field $\mathbf{B}_z$(F1) generated by μ_z(F1) weights this orbital current, which leads to the energy density ρ_{zz}(*x*SO). (c) For the SD term, each Cartesian component *j* (*j* = *x*, *y*, *z*) of $\mathbf{B}_z$(H2) generates a spin polarization subcomponent m_{zj}(SD)$\mathbf{n}_j$. These spin polarization subcomponents are weighted by the corresponding components of $\mathbf{B}_z$(F1) to form the subcomponents $\rho_{(zj)}$(SD), the SD energy density.

hybrid functional BLYP(60:40),[9] which combines 60% exact exchange and 40% Becke exchange[41] and uses for correlation exclusively the Lee−Yang−Parr correlation functional.[42] A suitable basis set for the calculation of ^1J(FH) was derived from Dunning's aug-cc-pVTZ basis[43] by (a) decontracting the innermost s basis function, (b) adding four compact s primitive Gaussian-type functions (GTFs) for each element in an even-tempered way (starting from the most compact s-type GTF in the standard cc-pVTZ basis set with a ratio of 6), and (c) deleting the diffuse functions with the highest angular momentum

TABLE 2: J-OC-PSP2 Analysis of SSCC ^1J for FH, Its Ramsey Terms, Their Orbital Contributions, and Their Cartesian Components[a]

contribution		calculation[b]	FC	SD			PSO			DSO			tot. iso
				x (=y)	z	iso	x (=y)	z	iso	x (=y)	z	iso	
c	dir. Ramsey[c]	(1)								−45.4	89.8	−0.3	−0.4
	self-X												0.0
	sum									−45.4	89.8	−0.3	−0.4
bd	dir. Ramsey	(2)	846.9	−8.9	−31.1	−16.3	−65.9	0.0	−43.9	−28.1	17.7	−12.8	773.8
	self-X		1208.4	−9.0	−34.7	−17.6	−14.5	0.0	−9.7				1181.1
	sum		2055.2	−17.9	−65.7	−33.8	−80.4	0.0	−53.6	−28.1	17.7	−12.8	1954.9
lp σ	dir. Ramsey	(3)	−393.2	−1.4	−4.0	−2.3	60.1	0.0	40.1	1.4	8.7	3.8	−351.6
	self-X		−183.4	−0.8	−2.6	−1.4	10.1	0.0	6.7				−178.1
	sum		−576.6	−2.2	−6.7	−3.7	70.2	0.0	46.8	1.4	8.7	3.8	−529.7
lp π	dir. Ramsey	(4)	0.0	21.8	26.3	23.3	193.5	−14.6	124.1	0.5	27.4	9.5	157.0
	self-X		0.0	17.7	26.5	20.6	121.5	−8.2	78.2				98.8
	sum		0.0	39.5	52.8	43.9	315.0	−22.9	202.4	0.5	27.4	9.5	255.8
bd ← c echo								negligible					
bd ← c ext.	steric X[d]	(5) − (2) − (1)	−10.9										−11.3
lp σ ← c echo								negligible					
lp σ ← c ext.	steric X[d]	(6) − (3) − (1)	−53.9				0.5						−53.5
bd ← lp σ echo	1-deloc	(9) − (2)	56.3	−0.4	−1.9	−0.9	−1.0		−0.7				54.7
	steric X		69.3	−1.0	−4.0	−2.0	0.7		0.5				67.8
	sum		125.6	−1.5	−5.9	−3.0							122.5
bd ← lp σ ext	1-deloc	(7) − (9) − (3)	−319.1	−2.1	−8.2	−4.1	1.1		0.7				−322.5
	steric X		−763.0	−4.6	−18.3	−9.1	−1.0		−0.7				−772.8
	sum		−1082.1	−6.6	−26.5	−13.3							−1095.3
c ↔ bd ↔ lp σ	steric X	(8) − (7) − (6) − (5) + (1) + (2) + (3)	−132.5										−132.6
σ ↔ π	steric X[d]	(10)−(8)−(4)	30.0	3.5	4.1	3.7	13.2		8.8				42.5
Ramsey terms	dir. Ramsey + 1-deloc		190.7	9.1	−18.9	−0.3	188.0	−14.6	120.5	−71.5	143.7	0.2	311.1
	self-X + steric X		164.0	5.7	−29.5	−6.1	130.1	−8.2	84.0				241.9
	sum		354.8	14.7	−48.4	−6.3	317.9	−22.9	204.3	−71.5	143.7	0.2	553.0
expt[d]													555−566

[a] All values are given in Hz for the isotopes ^{19}F and ^{1}H. LMO contributions are denoted as c (core), bd (bond), and lp (lone pair). For the two-orbital contributions, the double-headed arrow indicates that both the contribution $B \rightarrow k \rightarrow l \rightarrow A$ and the contribution $A \rightarrow l \rightarrow k \rightarrow B$ is included. Here, "iso" denotes the isotropic average of the respective quantity, i.e., $J_{iso} = (2J_x + J_z)/3$. Values not shown in the table have an absolute value below 0.5 Hz. [b] The orbital contributions are calculated based on the following orbital configurations: (1) affff, (2) fafff, (3) ffaff, (4) fffaa, (5) aafff, (6) afaff, (7) faaff, (8) aaaff, (9) fapff, and (10) aaaaa. The five letters for each configuration specify the status of the individual orbitals (a = active, p = passive, f = frozen) in the order c−bd−lp(σ)−lp(π_x)−lp(π_y). [c] dir. Ramsey = direct Ramsey response, self-X = self-exchange, 1-deloc = first-order delocalization, and steric X = steric exchange interaction. The DSO term is considered a part of the direct Ramsey response in this context. [d] The 1-deloc terms are zero or negligible for these orbital contributions. [e] The experimental values correspond to the measured SSCC of 529 Hz[47] corrected for the vibrational contributions, which vary between 26 and 37 Hz.[35]

quantum number. The basis set obtained in this way is of (15s6p3d1f/10s3p1d)[15s4p3d1f/10s3p1d] quality and leads to a significant improvement of SSCCs involving fluorine as one of the coupling nuclei.

The J-**OC**-PSP*n* analysis[22,23] at level $n = 2$ and the orbital-selected SSCC calculations were carried out for LMOs obtained with a Boys localization[44] where however core, σ-, and π-orbitals are separately localized for reasons described elsewhere.[22] The orbital contributions were decomposed into direct Ramsey and self-exchange contributions (one-orbital terms) or into first-order delocalization and steric-exchange interaction terms (two- and more-orbital terms) with the method described in ref 34. All discussions are based on the bond σ(FH), the σ-(lone pair), the π(lone pair), and the core 1s(F) LMO. For the FH bond length the experimental r_e value of 0.9169 Å[45] was used.

The ^1J(FH) coupling constant is calculated for a total of 10 different orbital configurations: (1) affff, (2) fafff, (3) ffaff, (4) fffaa, (5) aafff, (6) afaff, (7) faaff, (8) aaaff, (9) fapff, and (10) aaaaa. Here the five letters for each configuration describe the status of the individual orbitals (a = active, p = passive, f = frozen) in the order c−bd−lp(σ)−lp(π_x)−lp(π_y). From these configurations, the J-**OC**-PSP2 contributions are derived as differences, as is shown in detail in Table 1.

Ramsey densities and selected orbital contributions to these densities are represented in form of contour line diagrams, where the contour levels are given by a geometric progression with a ratio of $100^{1/5}$ between two subsequent contours. All SSCC calculations and the J-**OC**-PSP analysis are performed with the ab initio program package COLOGNE2004.[46]

4. Application of the J-OC-PSP Method to the SSCC ^{1}J(F-h)

We will discuss in the following typical features of the spin−spin coupling mechanism in FH as they are reflected by the J-**OC**-PSP methods. We simplify the notation by using the symbols ^{n}X(AB) with X = FC, SD, PSO, DSO rather than $^n J^X_{A,B}$ for the Ramsey terms. In the same way, we will use X(LMO) rather than $^n J^{X,LMO}_{A,B}$ given that we consider a diatomic molecule.

The measured SSCC ^1J(FH) is 529 Hz (value obtained for the gas phase[47]), which has to be corrected for a calculated vibrational contribution of 26 to 37 Hz (depending on the method used)[35] thus leading to a value of 555 to 566 Hz, which is in reasonable agreement with the calculated value of 557 Hz (Table 2). Clearly, XC functional and basis set have to be fine-tuned to reproduce a value as close as possible to the experimental value and to get in this way Ramsey terms and orbital contributions that, if summed up, reproduce the experimental value. However, we have also employed the standard B3LYP[48] and two other functionals in connection with with smaller basis sets used in previous work[9,22] for testing purposes. Although the calculated ^1J(FH) values differ by more than 200

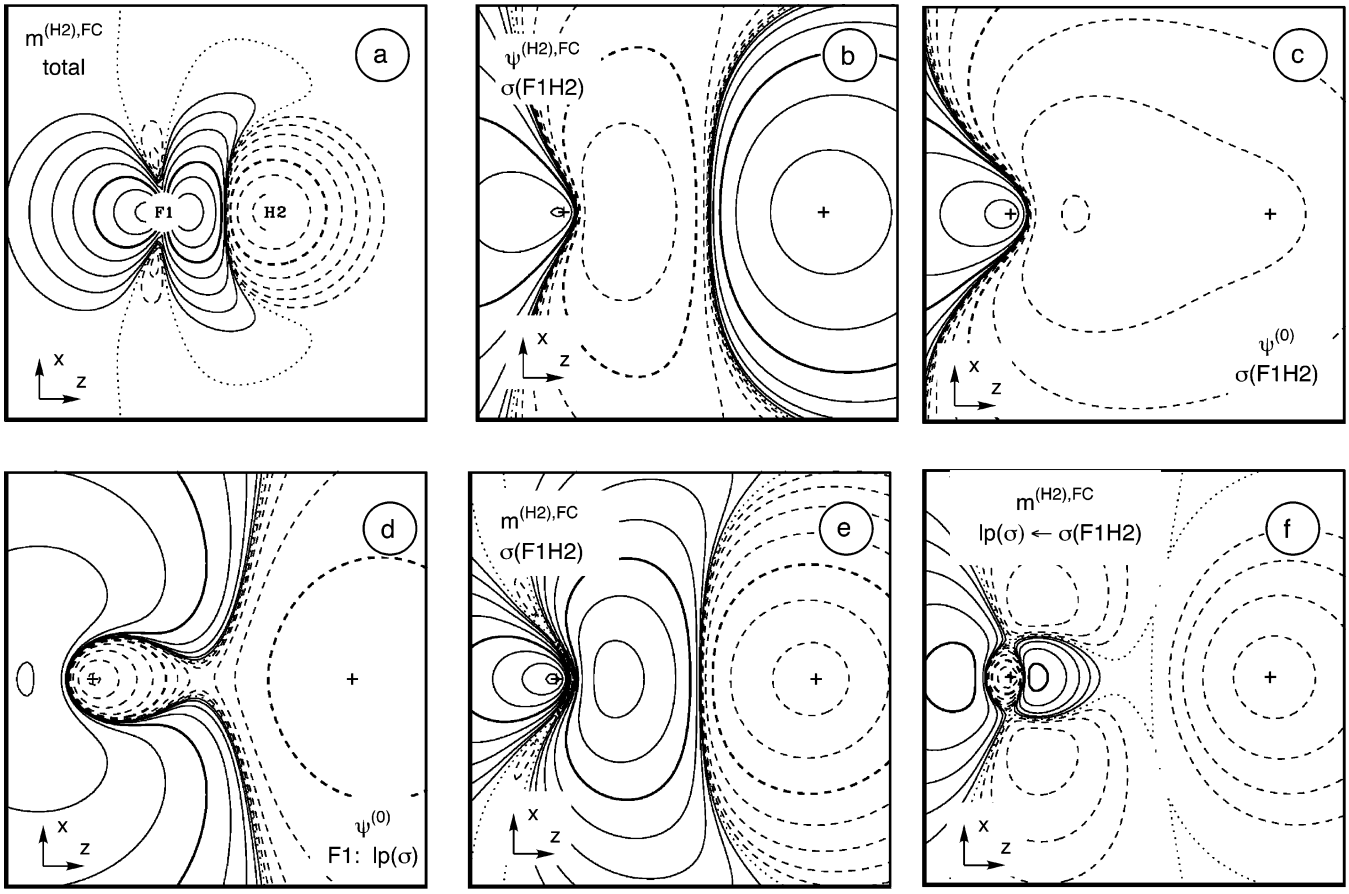

Figure 2. Analysis of the FC term of the SSCC ^1J(FH) calculated at the CP-DFT/BLYP(60:40) level of theory. (a) Total FC spin density distribution. (b) First-order bond orbital for the one-orbital contribution FC(bond orbital). (c) Zeroth-order bond orbital. (d) Zeroth-order lone-pair(σ) orbital. (e) FC spin density distribution for the one-orbital contribution FC(bond orbital). (f) FC spin density distribution for the one-orbital contribution FC(lone pair). The contour line diagrams are given for a plane containing the FH bond axis. Solid contour lines indicate a dominance of α spin density (positive amplitudes), dashed contour lines β spin density (negative amplitudes). The spin of the perturbing nucleus H2 is assumed to be α. Contour lines for 0.1 and 10 are printed in bold.

Hz from the experimental, vibrationally corrected value in these cases, the trends in the Ramsey terms and orbital contributions determined with the large basis set were largely reproduced with the smaller basis sets and the other functionals. Hence, we can conclude that the description obtained in this work is of general value.

Analysis of the FC Contributions. Figure 2a gives the total FC spin density distribution for the SSCC ^1J(FH). The *xz*-plane is the drawing plane, with the FH bond being oriented along the *z* axis. The H nucleus is the perturbing nucleus, for which α nuclear spin is assumed. Consequently, there is a dominance of β electron spin surrounding the H nucleus (dashed contour lines in Figure 2a). In the bond region, there is a nodal surface and the FC spin density distribution around the F nucleus is positive (dominance of α electron spin). The J-OC-PSP analysis (Table 2) reveals that the one-electron bond (bd) orbital contribution (2055 Hz) to the FC term (corresponding to a Ramsey distortion) is positive and mainly responsible for the large positive FC term.

Of the bd FC term, only 41% (847 Hz) are due to direct Ramsey response whereas 59% (1208 Hz) result from self-exchange interaction. The portion of the self-exchange interaction is thus higher than, e.g., for ^{1}FC(CH) in CH_4 (43%, ref 34). Due to the high electronegativity of the F atom, the bd orbital is strongly distorted toward F thus establishing a polar bond (see Figure 1c). Accordingly, the bd orbital is relatively difficult to deform by a direct Ramsey response. In addition, the Coulomb interaction between α and β electron is large, which gives rise to an intense self-exchange interaction once the centroids of α and β electrons have been shifted against each other by an external perturbation. This indicates that there is a relationship between the self-exchange part of the bd contribution and the electronegativity difference between the atoms involved: For a polar bond, the bond orbital will be compact with a large repulsion between the α and β electron in the orbital, which facilitates a strong self-exchange interaction. The direct Ramsey response, in contrast, is related to the polarizability of the molecule: If it is easy to deform the orbital by a homogeneous external field, then it will be likely that the orbital will react sensitively to the perturbing nucleus as well.

The bd contribution (FC Ramsey distortion) is partly compensated for by the negative one-orbital contribution from the lone pair (lp) orbital of −577 Hz. It should be noted that this contribution arises solely from the lp(σ) orbital because the lp(π) orbitals make no active contributions. The opposite sign of the bd and lp one-orbital contribution is easy to rationalize by considering the zero- and first-order orbitals for a perturbation at H: Both the first-order bd (Figure 2b) and the first-order lp orbital (not shown) are dominated by the σ^*(FH) orbital, which has two nodal surfaces between F and H (one through the core region of F on the side of the bond, one in the F−H bond region). The zeroth-order bd orbital (Figure 2c) has just one nodal surface between F and H (passing through the bond close to F, Figure 2c), in contrast to the zeroth-order lp orbital (Figure 2d), which has no nodal surface between F and H (there is one behind the F nucleus in the lp region, Figure 2d). The FC density

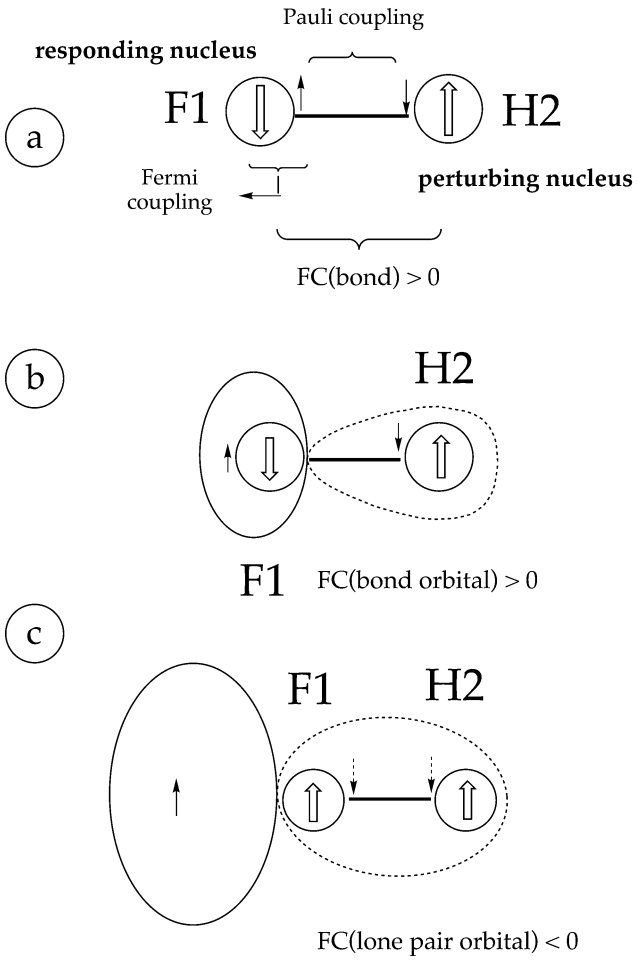

Figure 3. Dirac vector models of (a) FC(F−H) coupling, (b) the bond (bd) LMO contribution, and (c) the lone pair LMO contribution to ^{1}FC(F1H2). Large arrows indicate α- and β-spin of perturbing and responding nucleus, small arrows α- and β-spin of the electron. The perturbing nucleus is H2, which is assumed to always have α-spin and which is the starting point of the FC spin polarization. Solid arrows refer to specific electrons whereas dashed arrows indicate the spin density distribution rather than belonging to single electrons. The diffuse back lobes of the hybrid orbitals are indicated by dashed ellipses. Note that only the spin density at the position of the nuclei is schematically represented, however not that in other parts of the molecule, which is too complicated to be represented by simple Dirac models.

for a certain orbital is just twice the product of the corresponding zeroth- and first-order orbital. Thus, the FC spin density generated by the bd orbital (Figure 2e) has opposite signs at nucleus H (negative) and nucleus F (positive), whereas that from the lp orbital (Figure 2f) has equal signs at the coupling nuclei (both negative). According to the Dirac vector model (Figure 3), this implies a positive contribution to the ^{1}FC(FH) term from the bd and a negative one from the lp orbital.

The portion of self-exchange interaction is 32%, i.e., smaller for the lp(σ) than for the bd orbital. The bd orbital is located axially around the FH bond, whereas the lp(σ) orbital is concentrated around the F atom and stretches outside the FH bond. Consequently, the α−β electron repulsion in the lp(σ) bond is less effective in enhancing the perturbation generated by the external spin than it is observed for the bd orbital.

The Dirac vector model is normally used in a way similar to that shown in Figure 3a: Fermi coupling between the nuclear α spin and the surrounding electrons leads to a dominance of β electron spin at the contact surface of the perturbing nucleus. Pauli coupling of the electrons in the bond orbital generates α electron spin at the responding nucleus, which in turn adopts β spin. Taking Figure 3a as a schematic description for FC spin−spin coupling, one could conclude that Pauli pairing and perhaps even dynamic electron correlation are responsible for the transport mechanism of FC spin polarization from perturbing to responding nucleus. This however is not the case: Pauli pairing is already valid for the zeroth-order density and may be considered as the guarantee that there is 50% of α and 50% of β electron spin in the total molecule as well as in each LMO region. The transport of spin polarization is actually caused by the necessity of optimizing exchange interactions in the region of the perturbing nucleus B (here H2), which leads to a withdrawal of β electron spin out of the region of nucleus A (here F1) thus generating a dominance of α electron spin around A. Hence, *the maximization of stabilizing exchange interactions, rather than dynamic electron correlation, is indicated by the Dirac vector model*. Also, the information is given exclusively for the contact region and not for any other region in the valence shell or bond region. The sign of spin polarization can change several times according to the number and the positions of the nodal surfaces of zeroth- and first-order LMO in the molecule (compare parts e and f of Figure 2 with LMO pictures in parts b−d of Figure 2), which is not predicted by the Dirac vector model.

Keeping this in mind we use the Dirac vector model in a more general (extended) way to predict the sign of individual LMO contributions to the FC term. First, we consider the distribution of spin in an LMO. The lobe surrounding perturbing (and possibly responding) nucleus is the region of β electron spin, the back lobe the region of α electron spin. Next the position of the responding nucleus with regard to the nodal surface is determined. For bond LMOs in XH_n molecules the heavy atom X is always positioned in the rear lobe and for lp LMOs both X and H are positioned in the rear lobe of the lp orbital. Since the first-order orbitals for both bd and lp LMO have similar nodal structures, it is easy to verify the signs of the one-orbital contributions in the way shown in Figure 3, parts b and c. Because of the regular structure of the nodal patterns of zeroth- and first-order orbitals, the Dirac vector model is generally applicable for a class of orbital contributions once the FC spin density distribution or the nodal pattern is known. The latter has however to be verified for each new class of FC orbital contributions. Also, there is no way to predict the sign of the total FC term from the Dirac vector models of all orbital contributions. In so far its success in connection with the FC coupling terms of regular hydrocarbons has to be considered as an exception.

In the case of ^{1}FC(FH), the absolute value of the lp contribution is smaller than that of the bd contribution (Table 2) because of the lower density of the former at the H nucleus. On the other hand, the ratio between lp and bd contribution is larger for ^{1}FC(FH) (about 1:3) than for any of the other SSCC ^{1}FC(XH) involving first-row hydrides (NH_3: about 1:12, see ref 22). This is a consequence of the high electronegativity of F (higher spin density of the lp electrons at the contact surface of F and depletion of spin density at H, which results mainly from the polarity of the FH bond orbital).

The largest contribution from the lp orbital is its external bond contribution in connection with the bd orbital, which amounts to −1082 Hz and is to some extent compensated by an echo effect of 126 Hz. The bd and lp(σ) orbitals penetrate each other intensely in the region around the F atom. This makes a strong two-orbital interaction between bd and lp(σ) possible, especially by steric exchange interactions. This is also why the external

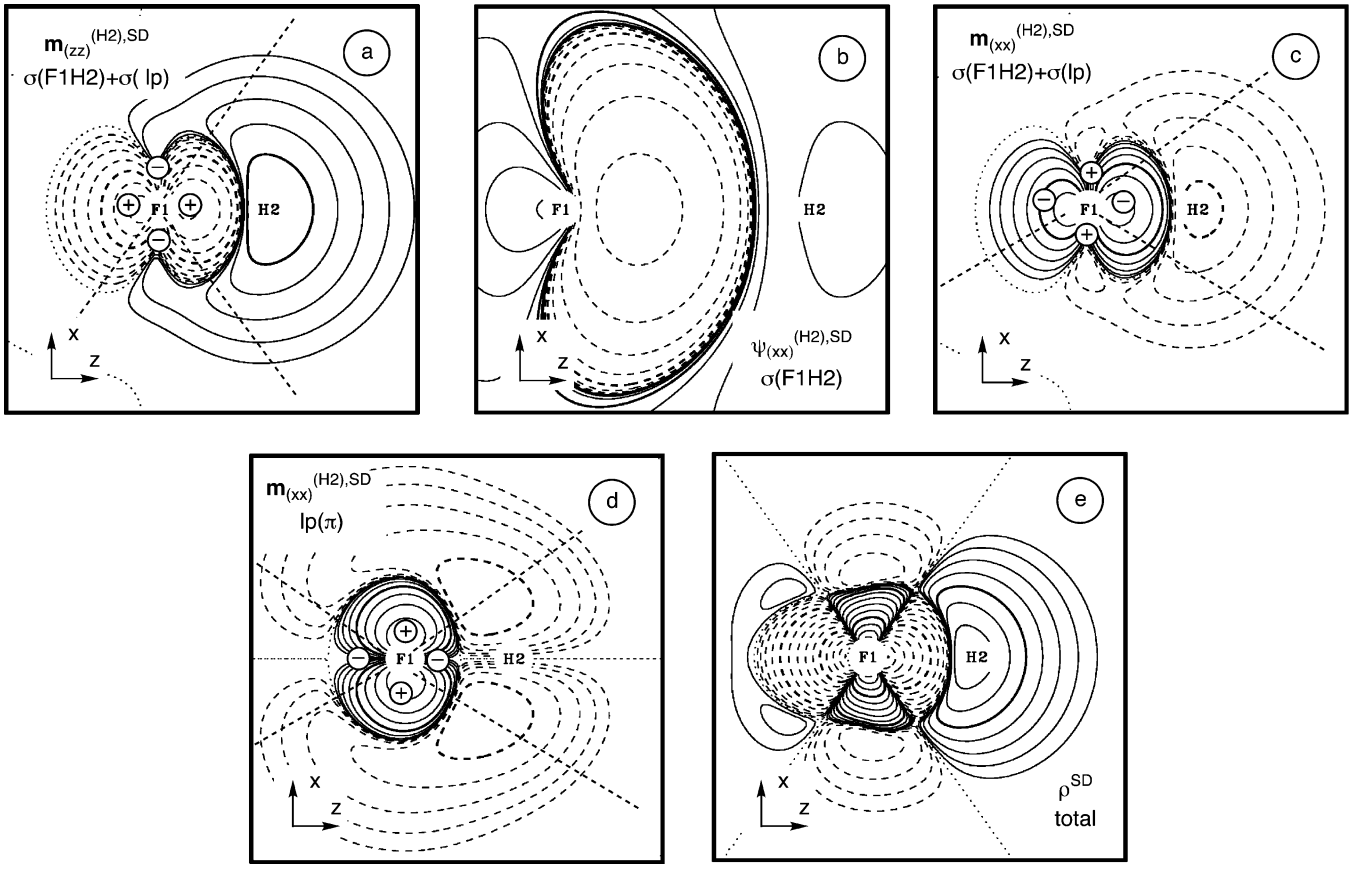

Figure 4. Analysis of the SD term of the SSCC ^1J(FH) calculated at the CP-DFT/BLYP(60:40) level of theory. (a) SD spin density distribution of the (*zz*) subcomponent for the contribution from the bond and lone-pair(σ) orbitals. (b) SD first-order orbital σ(FH) calculated for the (*xx*) subcomponent. (c) SD spin density of the (*xx*) subcomponent for the contribution from the bond and lone-pair(σ) orbitals. (d) SD spin density of the (*xx*) subcomponent for the contribution from the lone-pair(π) orbital, scaled by a factor of 10. (e) Isotropic SD energy density distribution, scaled by a factor of 10. In the case of the SD spin density distribution the orientation of the quadrupolar potential at the responding nucleus is indicated by dashed lines and appropriate ± signs. The contour line diagrams are given for a plane containing the FH bond axis. Solid (dashed) lines refer to α (β) surplus spin densities, positive (negative) amplitudes, or positive (negative) energy densities. The spin of the perturbing nucleus H2 is assumed to be α. Contour lines for 0.1 and 10 are printed in bold.

orbital contribution of the lp(σ) orbital is dominated by steric exchange interaction (71%), whereas the external orbital contribution for ^{1}FC(CH) in CH_4 contains only 19% steric exchange interaction.[34] As schematically indicated in Figure 3b, the spin polarization of the bd orbital generates an α spin surplus and consequently an α-attractive extra exchange potential in the region of the F atom. Due to the form of the bd orbital (Figure 2c), this potential is concentrated in the valence and bond region and nearly vanishes in the core region of F (the nodal surface of the bd orbital passes through the core region). This means that the electrons in the lp orbital are spin polarized in the way that α surplus density is withdrawn from the core region of F, leaving a β surplus there, which eventually makes a large negative contribution ^{1}FC(lp ← bd) to the FC term. This dominates a much smaller positive ^{1}FC(bd ← lp) contribution and leads to the negative ^{1}FC(bd ↔ lp) term. The same mechanism applies to the ^{1}FC(c ← bd) and ^{1}FC(c ← lp) contribution (the ^{1}FC(bd ← c) and ^{1}FC(lp ← c) terms are very small due to the localized character of the core (c) orbital) thus yielding ^{1}FC(c ↔ bd) and ^{1}FC(c ↔ lp) contributions of −11 and −54 Hz, respectively (Table 2).

The three-orbital interaction between c, bd, and lp(σ) orbital contributes −132 Hz to the FC term. Usually, three- and more-orbital paths make only small contributions to the total FC term. The large term encountered here is due to the fact that all three of the orbitals involved are concentrated in the region around the F nucleus and, accordingly, penetrate each other. This allows for an effective three-orbital spin transport where at least one of the orbitals acts as a passive orbital, e.g the lp orbital in the way that it passes spin information from the bd to the c orbital. This interaction is to be regarded as a combination of echo and external-orbital contributions.

Analysis of the SD Contributions. The total ^{1}SD(FH) term is relatively small (−6 Hz, see Table 1) because orbital contributions cancel each other largely. The σ orbitals (bd and lp) make negative contributions to the SD term, whereas the positive contributions arise from the lp(π) orbitals.

The interaction between the responding (perturbing) nucleus and the electron system takes place for the SD term nonlocally. The perturbing nuclear moment of H will generate a dipole field that is monitored by the quadrupolar potential residing at the responding nucleus F. For the purpose of understanding the SD coupling mechanism, first the subcomponents of the SD spin density are considered and then the SD energy density leading to the actual SD terms will be discussed.

Figure 4a gives the $m_{(zz)}^{(H2),SD}$ subcomponent of the SD spin density resulting from the σ(*bd*) and σ(*lp*) orbitals, i.e., the z component of the spin polarization for the perturbing moment at the H nucleus being in the *z* direction. Figure 4c shows the (*xx*) subcomponent of the SD spin density for the same two orbitals. The spin density distributions resemble each other apart from the opposite signature. Besides, the (*xx*) subcomponent resembles the FC spin density arising from the two σ orbitals

SCHEME 2: Schematic Representation of the $SD_{(zz)}$ Spin Polarization around the F Nucleus for a Perturbation in the *z*-Direction Considering Different Excitations (a and b)[a]

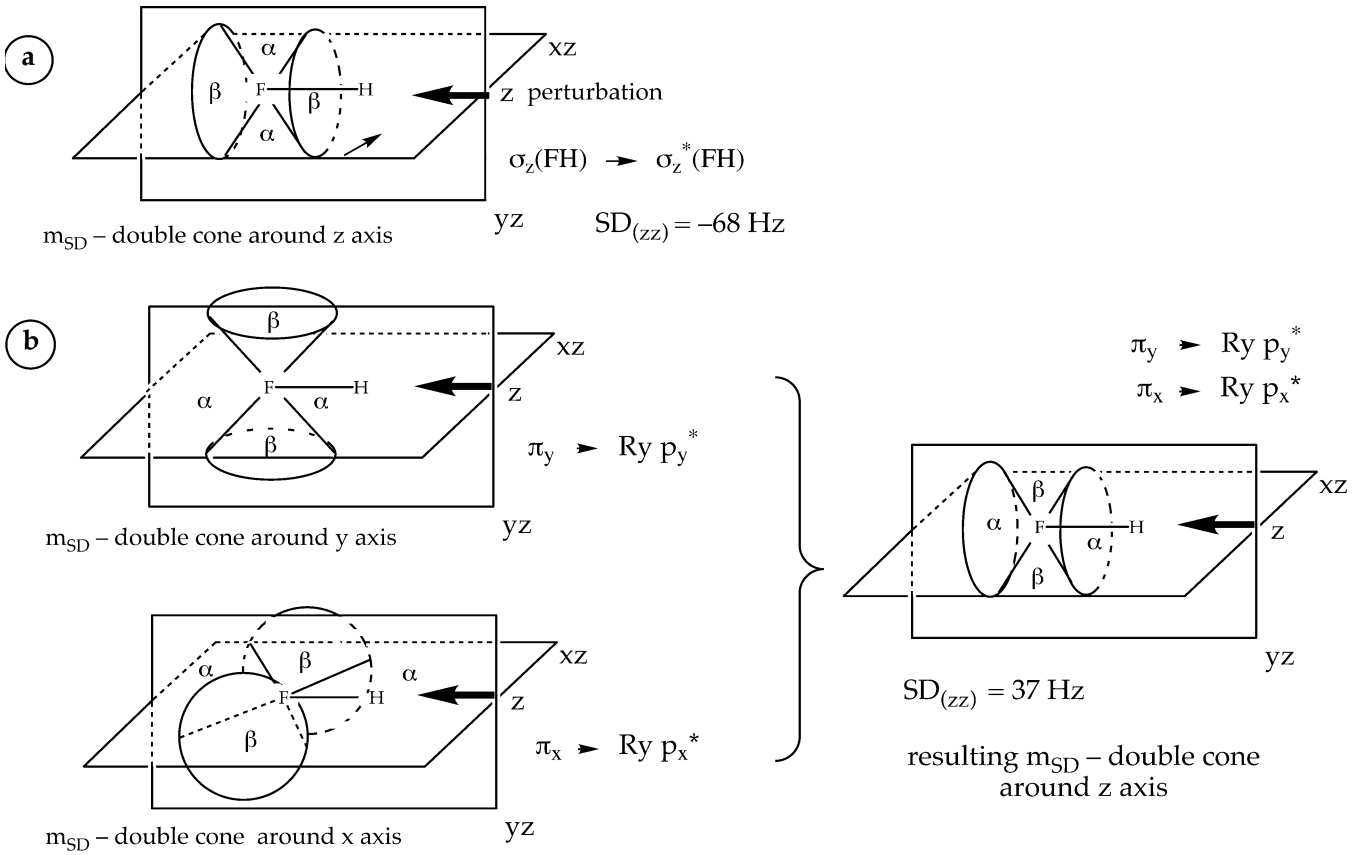

[a] The (*zz*) subcomponents are the leading terms of the *zz* components, which are −66 Hz (a) and 53 Hz (b).

(not shown). This suggests that the SD spin−spin coupling mechanism for the σ orbitals, analogously to the FC coupling, is dominated by excitations into the σ^*(FH) bond orbital as is confirmed by the plot of the first-order bd orbital for the (*xx*) subcomponent of the SD spin density (Figure 4b). The first-order orbitals for the SD(*xx*) and the FC term (Figure 2b) are similar to each other, the main difference being that the first-order orbital for the FC term has a larger s character at the H nucleus in response to the localized FC perturbation.

Scheme 2a shows schematically the form of the $m_{(zz)}^{(H2),SD}$ subcomponent generated by the bd orbital; the same qualitative picture applies for the $m_{(zz)}^{(H2),SD}$ contributions from the lp(σ) orbital and the bd ↔ lp(σ) interactions. The SD(*zz*) subcomponent from the bd contribution amounts to −68 Hz and dominates thus the contribution of this orbital to SD_z (66 Hz, Table 2). Both the σ(FH) and the σ^*(FH) orbitals have partial p_z character at both nuclei. The nodal surface of the spin polarization close to the F nucleus has the form of a double cone around the *z* axis, with the axial region having β surplus density. This spin polarization gives rise to a negative SSCC contribution, as can be seen from the signature of the quadrupole potential generated by the responding nucleus (see Figure 4a). Note that the (*xx*) and (*zz*) subcomponents from the σ orbitals both make negative contributions to ^{1}SD because the resulting spin polarization and the potential of the responding nucleus change their signatures (see Figure 4, parts a and c).

The π orbitals participate in the SD coupling mainly by excitations into high-lying Rydberg p-orbitals with some FH-antibonding π^* character. The (*xx*), (*yy*), and (*zz*) subcomponents all make positive contributions to ^{1}SD (2 × 40 and 53 Hz, respectively). Figure 4d shows the SD spin density for the (*xx*) subcomponent of the SD density related to the two lp(π) orbitals. The spin orientations are opposite around the H and the F atom, which reflects the nodal surface in the Rydberg p-orbital with π^* character.

It appears surprising that the main contribution to ^{1}SD from the lp(π_x) and lp(π_y) orbitals is in the (*zz*) subcomponent. Scheme 2b explains schematically how this contribution comes about: The perturbing nucleus H effectively generates excitations lp(π_x) → Ryd p_x and lp(π_y) → Ryd p_y, which is in line with the selection rules for the SD term.[26] The responding contributions to $m^{(H2),SD}$ are close to the F nucleus approximately double-cone shaped, the axes of the double cones being in *x* and *y* directions, respectively (Scheme 2b, left part). The resulting spin polarization is axially symmetric around the *z* axis (right part of Scheme 2b) thus leading to a (*zz*) subcomponent.

The form of the isotropic SD energy density (Figure 4e) can be rationalized considering the SD spin density distributions in Figure 4, parts a, c, and d, and taking into account the signatures of the weighting factors (resulting from the quadrupolar potential at the responding nucleus) also shown in these figures. All three SD spin densities shown make negative contributions to the SD energy density in the σ region around the F atom: The SD spin density in Figure 4a is negative and gets a positive weight, the density in Figure 4, parts c and d, are positive and get a negative weight. In the same way, the positive energy density in a torus around F as well as around and beyond the H nucleus can be understood. Generally, the SD energy density is more concentrated around the F nucleus than the SD spin densities, which reflects the r_A^{-3} weighting in $h^{(A),SD}$:

$$h_A^{SD} = \alpha^2\left[3\frac{(\mathbf{s}\cdot\mathbf{r}_A)\mathbf{r}_A}{r_A{}^5} - \frac{\mathbf{s}}{r_A{}^3}\right] \quad (2)$$

Here, the position of nucleus A is given by vector $\mathbf{R}_A$, the vector $\mathbf{r}_A = \mathbf{r} - \mathbf{R}_A$ defines the position and distance of an electron relative to nucleus A, α is Sommerfeld's fine structure constant, s is the electron spin in units of $\hbar$, and atomic units are used to simplify eq 2.

The positive and negative contributions from the SD energy density largely cancel each other, which supports the picture that the relatively small SD term results from a cancellation between large contributions with opposite sign.

Analysis of the PSO contributions. The spin−spin coupling mechanism in FH is peculiar in the way that the PSO term (204 Hz, Table 2) is of similar magnitude as the FC term (355 Hz). In the case of hydrocarbons, the FC term is dominating whereas the remaining terms often cancel each other to a large degree. The sizable PSO contribution is due to its x and y components, which are 317 Hz each, whereas the z component is −23 Hz. The J-**OC**-PSP analysis reveals that the leading isotropic contribution to the PSO term arises from the lp(π) orbitals (202 Hz, Table 2). Besides this, there are additional nonnegligible contributions from the bd (−54 Hz) and lp(σ) orbital (47 Hz), which largely cancel each other. The only isotropic two-orbital contribution above 1 Hz arises between the σ and π lp orbitals (9 Hz, Table 2).

Figure 5a shows the first-order orbital for the lp(p_x) orbital and the perturbation in y direction. This orbital is also dominated by the σ*(FH) orbital and, therefore, resembles the first-order orbitals shown in Figures 2b and 4b. The lp(p_x) first-order orbital has regions with a large gradient in z direction close to both nuclei, i.e., nodal surfaces passing close to the nuclei lead to distinct p_z character at both F and H. This explains why this orbital is effective for the PSO spin−spin coupling mechanism: The PSO mechanism is based on excitations of the form ($p_x \rightarrow p_y^*$) or ($p_y \rightarrow p_x^*$) for the *zz* term, ($p_x \rightarrow p_z^*$) or ($p_z \rightarrow p_x^*$) for the *yy* term, ($p_y \rightarrow p_z^*$) or ($p_z \rightarrow p_y^*$) for the *xx* term.[27] Excitations lp(π_y) → σ*(FH) and lp(π_x) → σ*(FH) can add substantially to the PSO term. Figure 5b shows the PSO current density $\mathbf{j}_x(r)$ for the lp(p_y) orbital, which gives evidence of a ring current around the F nucleus in the *yz* plane. In Scheme 3a, this ring current is schematically given by two circles and direction arrows attached to them to facilitate the reading of Figure 5b. As the corresponding PSO energy density in the *yz* plane (Figure 5c) reveals, this ring current gives rise to a region with a large positive PSO energy density around the F nucleus, which leads to an *xx* component of 315 Hz (Table 2). In Scheme 3b, it is indicated that the same value has to be obtained for the *yy* component.

Figure 5d depicts the first-order orbital for lp(π_y) and the perturbation being in z direction (See also Scheme 3c). Since the first-order orbital takes the form of a d-orbital, which is strongly concentrated around the F atom, the matrix element between zeroth- and first-order π orbitals at the H nucleus is small. Furthermore, the first-order orbital has a nodal surface close to the F nucleus (yielding to oppositely oriented ring currents next to F; see Scheme 3c), which means that the positive and negative contributions to the PSO energy density PSO_{zz} arising from the lp(π) orbitals largely cancel (Table 2, Scheme 3c).

Figure 5e gives the PSO current density for the bd and lp(σ) orbital and the perturbation being in x direction. One sees that the PSO current density is relatively weak and there is also no distinct ring current around the F nucleus. The corresponding first-order orbitals, which have p_x character, are similar to that shown in Figure 5d. The small total contribution from the σ orbitals is largely due to mutual compensation. The isotropic PSO energy density (Figure 5f) is dominated by the positive contributions from the lp(π) orbitals shown in Figure 5c.

The two-orbital contributions to the PSO term relative to the one-orbital terms are smaller than for the FC and SD terms. Generally, steric interactions are much weaker for the PSO than for the SD term as the orbital currents are not connected with a spin polarization but only an imaginary contribution to the exchange integrals. In standard DFT calculations, this contribution is largely suppressed because the XC functional does not depend on the electron current density. By using 60% of exact exchange in the XC functional employed for FH changes in the current density are much better described.

It is noteworthy that the lp(π) contribution to ^{1}PSO contains a nonnegligible portion (39%) of self-exchange repulsion. This term arises from the, compared to the resting electrons, different exchange interactions in the ring current. First-order delocalization interactions will be described correctly for the PSO term, independently of the XC potential chosen. However, the contribution of the delocalization interaction to the PSO term is small, mainly because of symmetry reasons.

It should be noted that the large role of the PSO term in FH results from an interplay of several factors: (1) The lp(π_x) and lp(π_y) orbitals together with the σ*(FH) orbital allow for an effective PSO coupling for the x and y orientations, which is not compensated for by the z component to any extent, as, e.g., in the case of acetylene.[27] (2) The FC coupling is comparably weak in FH. In reduced units, the FC(FH) coupling is only about 50% of the FC(CH) coupling in methane and about 10% of the FC(CC) coupling in acetylene.[9] This increases the relative contribution of the noncontact terms. (3) The high gyromagnetic ratios for ^{19}F and ^{1}H (25.1665 and 26.7522 × 10^7 rad T^{-1} s^{-1}, respectively[47]) convert the electronic coupling effects into large measurable SSCCs.

Analysis of the DSO Contributions. The DSO term is just 0.2 Hz (Table 2), where however a detailed analysis of ^{1}DSO(FH) either in terms of orbital contributions or in terms of Ramsey densities reveals that the small value is due to an effective cancellation of nonnegligible components. For FH, the lp orbitals contribute (3.8 + 9.5=) 13.3 Hz to ^{1}DSO(FH) which is nearly compensated by the bd contribution (−12.8 Hz) and the core contribution (−0.3 Hz, Table 2). The DSO energy density (Figure 6a) possesses a typical structure: All regions outside a circle around the FH bond (actually a sphere) add positively, all contributions inside the circle negatively[9] so that both contributions cancel largely yielding a small remaining positive ^{1}DSO(FH) value.

The bd orbital is mainly located inside the sphere whereas the lp orbital is concentrated outside the sphere. Figure 6b gives the DSO energy density of the bd orbital, which has to be seen from the side of the responding nucleus and weighted by $1/r^3$. Close to the F nucleus, the negative energy density in the bond region outweighs the positive energy density outside the bond region so that a negative ^{1}DSO(bd) value results. In the case of the DSO energy density of the lp (Figure 6c), the positive DSO energy density outside the bond outweighs the negative density so that a positive ^{1}DSO(lp) value results. As regards the nearly perfect cancellation of the orbital terms, it has been proven in ref 22 that a spherical charge distribution around one of the nuclei does not make a sizable contribution to the isotropic DSO term as long as the radius of this charge distribution does not exceed the bond length. For fluorine, both the core and the

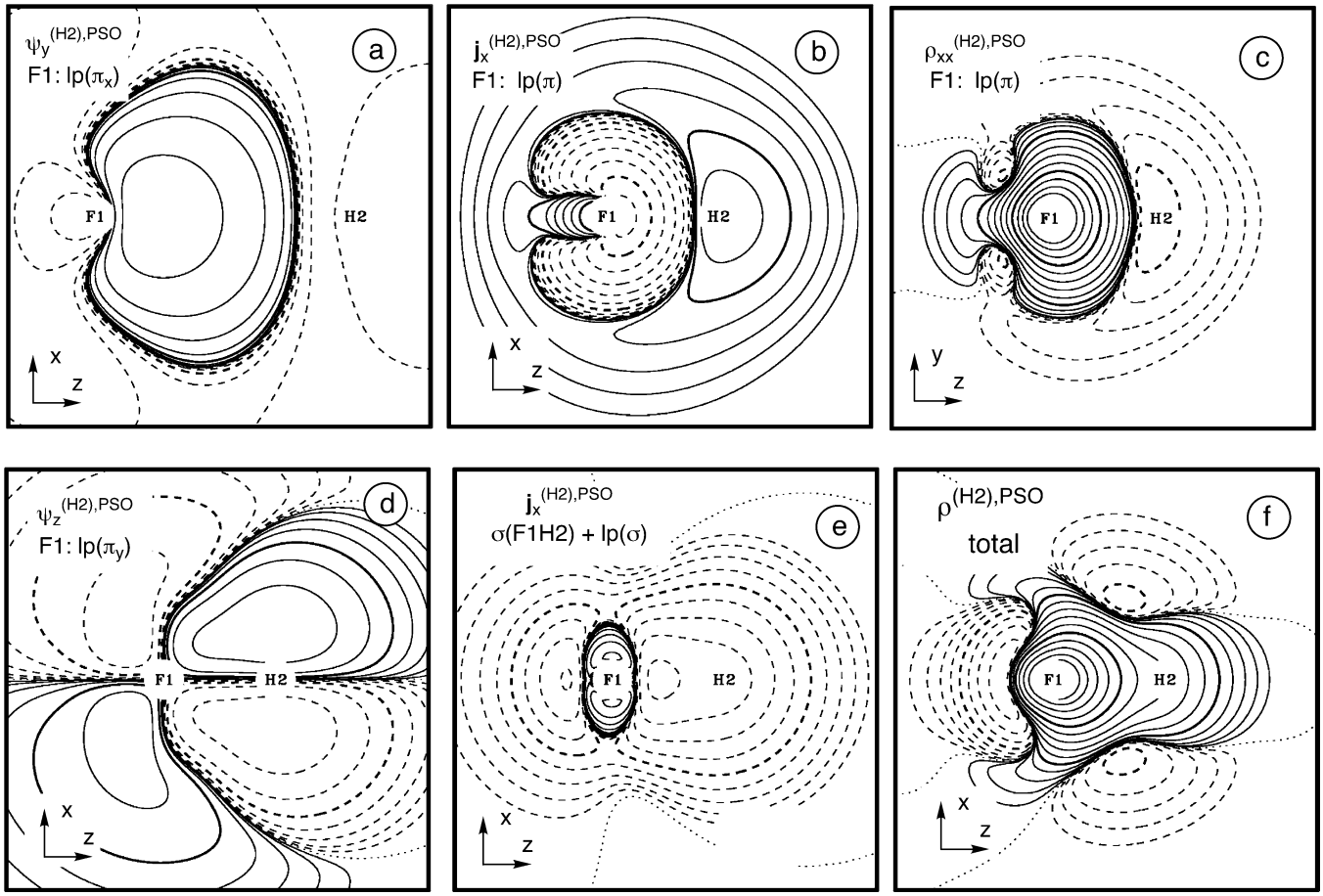

Figure 5. Analysis of the PSO term of the SSCC ^1J(FH) calculated at the CP-DFT/BLYP(60:40) level of theory. (a) PSO first-order orbital lp(p_x) given for the perturbation in *y* direction. (b) PSO current density distribution j_x^{PSO} for the two lp(π) orbitals in the *xy* plane leading to a current in the *yz* plane. (c) PSO energy density distribution ρ_{xx}^{PSO} shown in the *yz* plane. (d) PSO first-order orbital lp(π_y) for the perturbation being in z direction. (e) PSO current density j_x^{PSO} for the bd and lp(σ) orbitals and the perturbation being in the *x* direction. (f) Isotropic PSO energy density distribution. The contour line diagrams are given for a plane containing the FH bond axis. Solid (dashed) lines refer to positive (negative) amplitudes, scalar densities or current densities out of (into) the drawing plane. The spin of the perturbing nucleus H2 is assumed to be α. Contour lines for 0.1 and 10 are printed in bold. All densities are scaled by a factor of 10.

valence shell as a whole are nearly spherical, which explains the small ^{1}DSO(FH) value.

It is noteworthy that the Cartesian components of the DSO term are not small: The Cartesian components for the core contribution are about +150 and −300 times, respectively, the isotropic average. For the total DSO term, the Cartesian components are in the same order of magnitude as for the PSO term, but there is a nearly perfect cancellation between the individual components. This is in line with the analysis in ref 9, where it has been shown that the small value of the DSO term is due to a nearly perfect cancellation between the Cartesian components.

5. NMR Spin−Spin Coupling as a Probe for the Electronic Structure of XH Molecules

This work has demonstrated how the J-OC-PSP analysis method combined with a visualization of the individual contributions to the SSCC (Ramsey terms, orbital contributions) in form of density distribution diagrams can be used to elucidate the spin−spin coupling mechanism in a detailed manner. From the analysis of NMR spin−spin coupling in FH, the following conclusions with regard to the electronic structure of the molecule can be drawn (compare with Figure 1).

The DSO term gives an insight into the overall electron density distribution in FH. The 1s electron is spherical with just little core polarization as reflected by the core contribution. The bond electron pair is tightly concentrated along the FH internuclear axis (small magnitude of *x* (=*y*) component, Table 2). The valence density distribution at F is also largely spherical, which leaves only the possibility of forming a strongly polar bond with F approaching the electronic structure of the F anion. For X = Cl, Br, and I, the DSO term becomes more positive because the electronegativity of X, by this polarity of the X−H bond, and the X^- character is reduced. Hence, a reliable DSO term, although in general small, can provide a useful insight into the overall-picture of the electronic structure.

The large lp(π) PSO contributions confirm the important role of these orbitals for the PSO coupling mechanism; however they would not be possible without a low-lying σ*(FH) orbital, which according to the selection rules is required for a strong orbital current in the *xz* and *yz* planes (Scheme 3, parts a and b). The decomposition of the PSO term provides two important pieces of information: (a) The σ*(FH) orbital is composed at F from a $2p_z$ orbital with little 2s character (otherwise the lp(π) contributions would be small). (b) This antibonding orbital will be the LUMO because all other PSO contributions are smaller by a factor of 5−10 and symmetry considerations in connection with the selection rules leave no other possibility. The fact that the lp(π) term is substantially enhanced by self-exchange interaction reveals that the magnetic perturbation gives rise to

SCHEME 3: Schematic Representation of the Orientation and Direction of the Orbital Currents (a) $j_x(r)$ in the *yz*-Plane, (b) $j_y(r)$ in the *xz*-Plane, and (c) $j_z(r)$ (Always Bold Circles with Small Arrows) in the xy-Planes Containing Perturbing Nucleus H2 and Responding Nucleus F1 for a Perturbation (Fat Arrow) in the *x*-, *y*-, or *z*-Direction, Respectively[a]

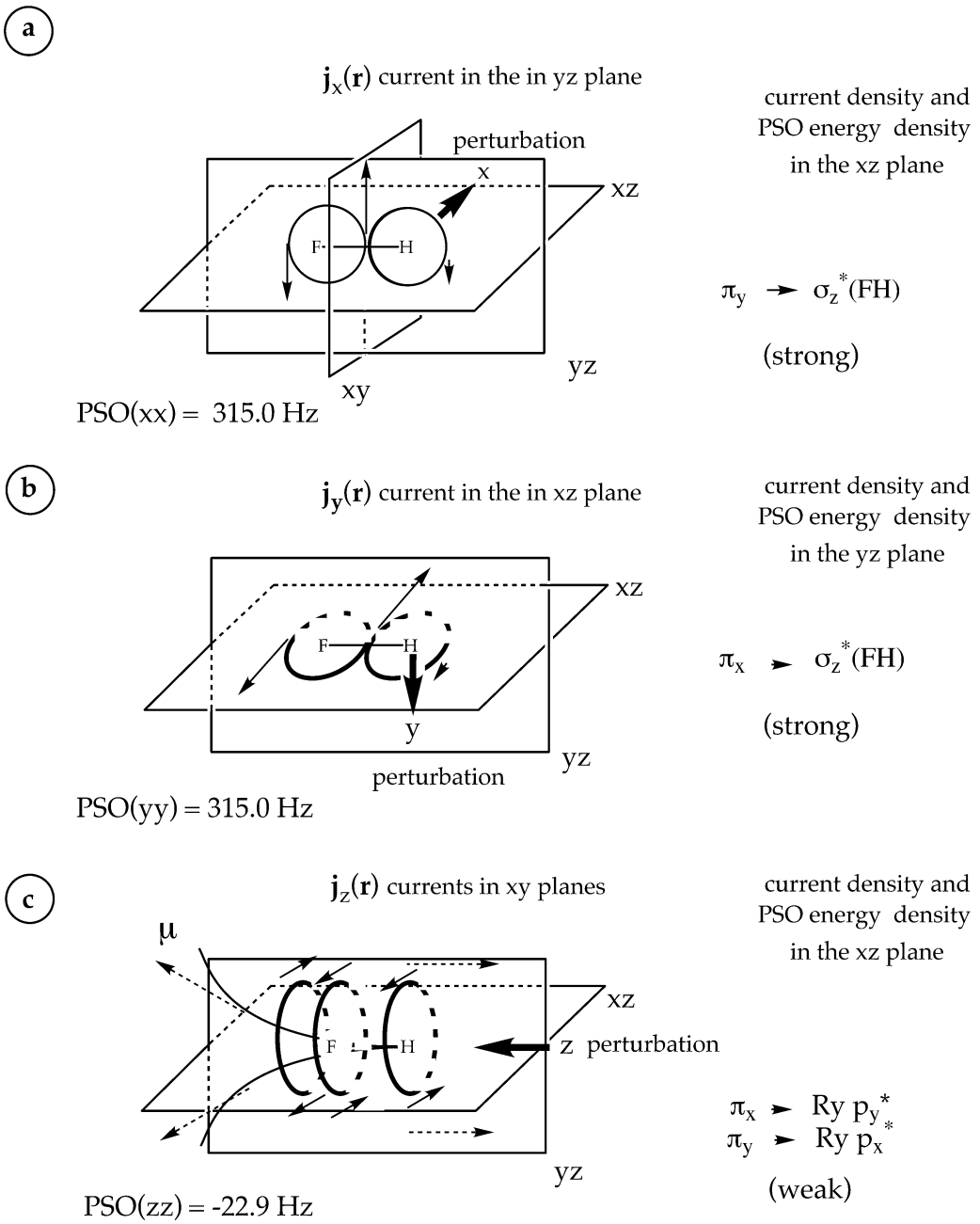

[a] The direction of the magnetic dipole field **B** is indicated by dashed arrows, the field lines by normal lines in part c. The dominating electron excitations and the PSO component values are given. Note that in the case of part c, there are two currents of opposite direction in the vicinity of F.

orbital currents in the lp(π) orbitals large enough to influence the self-exchange of the orbitals.

The SD contributions confirm and complement what has been found by the PSO contributions. Because the selection rules also include excitations with constant angular momentum quantum number,[26] a second hint on the existence of a low-lying σ^*(FH) orbital is given by the relatively large *z*-component of SD(bd), which is due to a σ(FH) $\rightarrow$ σ^*(FH) excitation. The value SD_{zz}(bd) is however just -72 Hz indicating that the σ-(FH) is also low in energy thus increasing the energy difference $\epsilon(\sigma(FH)) - \epsilon(\sigma^*(FH))$. The SD term also suggests that the Rydberg p-type MOs (3p, 4p, etc. of F) are too high in energy to lead to large SD(lp π) values.

Changes in the SD term can be predicted for the case that F is replaced by higher halogens X. If it is assumed for the moment that H and X are coupled by an isotropic polarizable medium then $^1SD_{xx} = {}^1SD_{yy} = -\,{}^1SD_{zz}/2$, i.e., $^1SD = 0$ in the isotropic average. This does not exclude that for any orientation of the perturbing nucleus the electron system is spin-polarizable and that each component of the SD term can be relatively large. In the case of X = F, the *zz* component is distinguished in that the σ^*(FH) has a relatively large amplitude at both nuclei whereas the lp π orbitals are concentrated around the F atom. Thus, SD coupling in *zz* direction is most effective and dominates the sum $^1SD_{xx} + {}^1SD_{yy}$ so that the isotropic SD term becomes negative (Table 2). For the halogen hydrides with

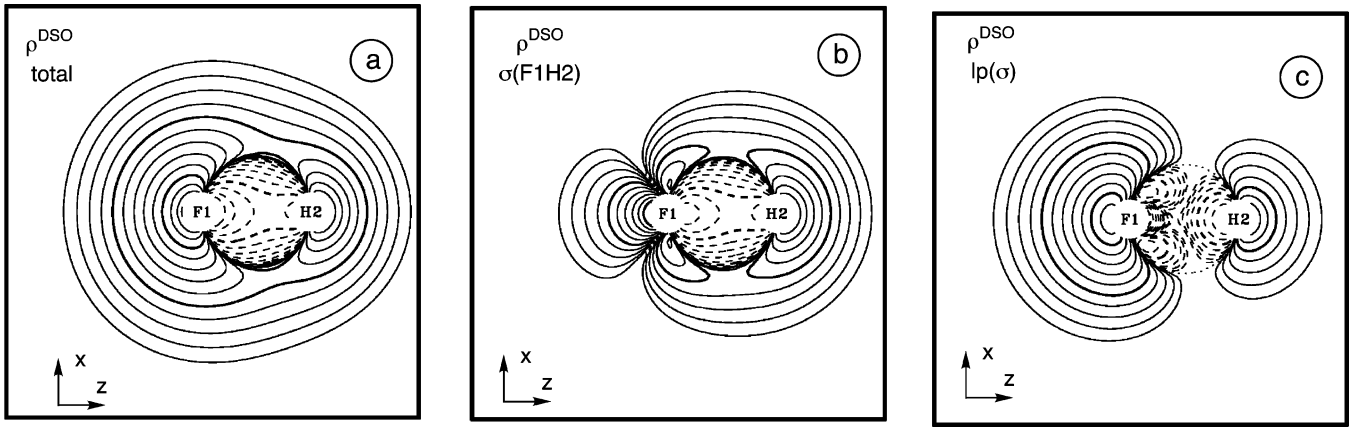

Figure 6. Analysis of the DSO term of the SSCC ^1J(FH) calculated at the CP-DFT/BLYP(60:40) level of theory. (a) Total isotropic DSO energy density distribution. (b) Isotropic DSO energy density distribution for the bond orbital. (c) Isotropic DSO energy density distribution for the lone-pair(σ) orbital. The contour line diagrams are given for a plane containing the FH bond axis. Solid (dashed) lines refer to positive (negative) DSO energy densities. The spin of the perturbing nucleus H2 is assumed to be α. Contour lines for 0.1 and 10 are printed in bold. All densities are scaled by a factor of 10.

X = Cl, Br, and I, the isotropic SD term becomes more positive[22] which indicates that the polarizability of the electron system in *x, y* direction increases more than in *z* direction. For increasing atomic number *Z*, the lp(π) orbitals are screened from the nuclear charge more and more, they become more diffuse, and the polarizability in *x, y* direction increases. The same holds, of course, also for the bd and lp(σ) orbitals, however these orbitals feel the nuclear charge of both X and H nucleus and therefore are less diffuse, i.e., the density in the *z*-direction is less polarizable. One can predict that for X = Cl (SD value close to zero[22]), the electron system of XH behaves to a large extent as an isotropic medium with regard to SD coupling.

The FC term provides insight into the properties of the σ-electrons of the XH molecule. The contribution ^{1}FC(bd) can be directly related to the nature of the XH bond. The self-exchange provides a measure for the bond polarity resulting from the electronegativity difference between the bonded atoms. The larger the self-exchange contribution is, the larger is the electronegativity of X and the charge transfer from H to X. The bond electron pair is confined to a relatively small space along the bond axis close to X and the relative shift in the centroids of α and β orbitals leads to a strong reduction of $\alpha-\beta$ electron repulsion combined with an equally strong increase in self-exchange. It is easy to predict that the self-exchange term becomes smaller in the series X = F, Cl, Br, and I due to the decrease in the electronegativity of X.

The direct Ramsey response of ^{1}FC(bd) depends on the polarizability of the bd density. This increases with increasing atomic number of X since the shielding effect of the core electrons also increases. The observed increase in ^{1}FC(bd) for X = F, Cl, and Br[22] clarifies that the bond polarizability (direct Ramsey response) dominates the bond polarity (self-exchange) for higher X. This is in line with the decrease in bond polarity due to the decreasing electronegativity of X and the enlarged atomic volume of higher X.

The different signs of ^{1}FC(bd) and ^{1}FC(lp(σ)) indicates the nodal structure of the zeroth-order orbital. For the bd orbital the nodal surface must be close to the F nucleus on the H side whereas for the lp(σ) orbital it is on the opposite side. This conclusion can be drawn because the corresponding first-order orbitals are dominated both by the σ*(FH) orbital (H is perturbing nucleus) and have the same nodal behavior. The ratio of self-exchange to direct Ramsey response reveals that lp(σ) is less contracted than the bd orbital and better polarizable than the bd orbital (Table 2).

Clearly, the polarizability of lp(σ) will increase in the series X = F, Cl, Br, I so that the lp-contributions become more and more negative. The same will be true for the external orbital contribution bd flp(σ) so that the FC term in total should become negative and ^1J(XH) should decrease. Exactly, this is found for the measured SSCCs.[22] It shows the importance of the lp orbitals for the spin−spin coupling mechanism, their role as external orbitals, and their increasing polarizability, which changes the value of ^{1}FC(XH). Since the lp(σ) and the bd ← lp σ contributions become more negative, at the same time the self-exchange part of the bd orbital is reduced, and only the direct Ramsey response of bd increases. There is an overall reduction of SSCC ^1J(XH) for increasing X. Or in short: ^1J(XH) becomes smaller because the electronegativity of X decreases and the polarizability of the lp electrons increases.

The relatively large negative two-orbital contribution bd → lp(σ) provides two pieces of information: (a) The participating orbitals overlap effectively (strong steric exchange) and (b) there is an antibonding orbital of relatively low energy, the σ*(FH) orbital, so that a significant first-order delocalization term can result. This confirms the special role of the σ*(FH) orbital as LUMO as already indicated by the PSO and the SD terms.

Summarizing the SSCC ^1J(FH) contains hidden information on the electronegativities of the coupling nuclei and thereby the bond polarity, the bond polarizability as well as the polarizability of the lone pair orbitals, the overlap between the σ-orbitals, the composition of the σ- and σ*-orbitals in terms of 2s(F) and 2p$_z$(F) character, the identification of the LUMO, the qualitative ordering of excited states, and the overall electron density distribution with regard to the X atom as center (X^--character), with regard to the bond sphere, or with regard to the lp-sphere. Most of these predictions may appear trivial because the electronic structure of FH is well-known. So far, however, it had not been known that electronic structure information normally collected from many different spectroscopic measurements can be extracted from a single NMR parameter provided the measured value is reproduced quantum chemically and analyzed as done in this work. Such a procedure would lead to completely new insights if applied to the higher HX with X = Br, I, and At, for which the electronic structure is not so clear. It would be also useful for the investigation of inter-halogen compounds XY or diatomic molecules in general.

After having a tool to identify those electronic effects responsible for the spin−spin coupling mechanism, the sign and the magnitude of the SSCC, it will be possible in the future to

use SSCCs in turn to describe the electronic structure, for more complex molecules and coupling situations than this was possible in the past. In this way a more complete description of chemical bonds by experimental means can be achieved, which includes especially through-space interactions between external orbitals of the bond considered (see Figure 1).

Acknowledgment. Calculations were done on the supercomputers of the Nationellt Superdatorcentrum (NSC), Linköping, Sweden. D.C. thanks the NSC for a generous allotment of computer time. J.G. thanks Carl Tryggers Stiftelse for financial support.

References and Notes

(1) See, e.g.: *Encyclopedia of Nuclear Magnetic Resonance*, Grant, D. M., Harris, R. K., Eds., Wiley: Chichester, U.K., 1996; Vols. 1−8, and references therein.

(2) Ramsey, N. F. *Phys. Rev.* **1953**, *91*, 303.

(3) (a) Kowalewski, J. *Prog. NMR Spectrosc.* **1977**, *11*, 1. (b) Kowalewski, J. *Annu. Rep. NMR Spectrosc.* **1982**, *12*, 81.

(4) For reviews, see (a) Helgaker, T.; Jaszunski, M.; Ruud, K. *Chem. Rev.* **1998**, *99*, 293. (b) Fukui, H. *Prog. NMR Spectrosc.* **1999**, *35*, 267.

(5) Oddershede, J. In *Methods in Computational Molecular Physics*; Wilson, S., Diercksen, G. H. F., Eds., Plenum Press: New York, 1992; p 303. (b) Wigglesworth, R. D.; Raynes, W. T.; Sauer, S. P. A.; Oddershede, J. *Mol. Phys.* **1997**, *92*, 77. (c) Wigglesworth, R. D.; Raynes, W. T.; Sauer, S. P. A.; Oddershede, J. *Mol. Phys.* **1998**, *94*, 851. (d) Enevoldsen, T.; Oddershede, J.; Sauer, S. P. A. *Theor. Chem. Acc.* **1998**, *100*, 275. (e) Wigglesworth, R. D.; Raynes, W. T.; Kirpekar, S.; Oddershede, J.; Sauer, S. P. A. *J. Chem. Phys.* **2000**, *112*, 3735.

(6) (a) Laaksonen, A.; Kowalewski, J.; Saunders: V. R. *Chem. Phys.* **1983**, *80*, 221. (b) Vahtras, O.; Ågren, H.; Jørgensen, P.; Jensen, H. J. A.; Helgaker, T.; Olsen, J. *J. Chem. Phys.* **1992**, *96*, 2118. (c) Vahtras, O.; Ågren, H.; Jørgensen, P.; Jensen, H. J. A.; Helgaker, T.; Olsen, J. *J. Chem. Phys.* **1992**, *97*, 9178.

(7) Perera, S. A.; Nooijen, M.; Bartlett, R. J. *J. Chem. Phys.* **1996**, *104*, 3290.

(8) (a) Gauss, J.; Stanton, J. F. *Chem. Phys. Lett.* **1997**, *276*, 70. (b) Auer, A. A.; Gauss, J. *J. Chem. Phys.* **2001**, *115*, 1619.

(9) Sychrovský, V.; Gräfenstein, J.; Cremer, D., *J. Chem. Phys.* **2000**, *113*, 3530.

(10) For independent CP-DFT developments, see: (a) Helgaker, T.; Watson, M.; Handy, N. C. *J. Chem. Phys.* **2000**, *113*, 9402. (b) Barone, V.; Peralta, J. E.; Contreras, R. H.; Snyder, J. P. *J. Phys. Chem. A* **2002**, *23*, 5607. (d) Peralta, J. E.; Barone, V.; de Azua, M. C.; Contreras, R. H. *Mol. Phys.* **2001**, *99*, 655. (e) Peralta, J. E.; de Azua, M. C.; Contreras, R. H. *Theor. Chem. Acc.* **2000**, *105*, 165.

(11) Contreras, R. H.; Facelli, J. C. *Annu. Rep. NMR Spectrosc.* **1993**, *27*, 255.

(12) (a) Contreras, R. H.; Peralta, J. E. *Prog. NMR Spectrosc.* **2000**, *37*, 321. (b) Contreras, R. H.; Peralta, J. E.; Biribet, C. G.; Ruiz De Azua, M. C.; Facelli, J. C. *Annu. Rep. NMR Spectrosc.* **2000**, *41*, 55.

(13) Contreras, R. H.; Barone, V.; Facelli, J. C.; Peralta, J. *Annu. Rep. NMR Spectrosc.* **2003**, *51*, 167.

(14) (a) Karplus, M.; Anderson, D. H. *J. Chem. Phys.* **1959**, *30*, 6. (b) Karplus, M. *J. Chem. Phys.* **1959**, *30*, 11.

(15) Karplus, M. *J. Am. Chem. Soc.* **1963**, *85*, 2870.

(16) For a recent review, see: Altona, C. In *Encyclopedia of Nuclear Magnetic Resonance*; Grant, D. M., Harris, R. K. Eds., Wiley: Chichester, U.K., 1996; p 4909.

(17) (a) Pople, J. A.; Schneider, W. G.; Bernstein, H. J. *High-resolution Nuclear Magnetic Resonance*; McGraw-Hill: New York, 1959. (b) Emsley, J. W.; Feeney, J.; Sutcliffe, L. H. *High-resolution nuclear magnetic resonance spectroscopy*; Pergamon: Oxford, U.K., 1966.

(18) Günther, H. *NMR Spectroscopy*; Thieme: New York, 1983.

(19) Kalinowski, H. O.; Berger, S.; Braun, S. *^{13}C NMR-Spektroskopie*; Georg Thieme Verlag: Stuttgart, Germany, 1984; and references therein.

(20) Webb, G. A. *Annual reports on NMR spectroscopy*; Academic Press: London, 1985−2002.

(21) (a) Barfield, M.; Chakrabarty, B. *Chem. Rev.* **1969**, *69*, 757. (b) Barfield, M. *Indirect Coupling: Theory and Applications in Organic Chemistry* in *Encyclopedia of NMR*; Wiley: New York, 1996; p. 2520.

(22) Wu, A.; Gräfenstein, J.; Cremer, D. *J. Phys. Chem.* **2003**, *107*, 7043.

(23) Gräfenstein, J.; Tuttle, T.; Cremer, D. *J. Chem. Phys.* **2004**, *120*, 9552.

(24) Tuttle, T.; Kraka, E.; Wu, A.; Cremer, D. *J. Am. Chem. Soc.* **2004**, *126*, 5093.

(25) Tuttle, T.; Gräfenstein, J.; Wu, A.; Kraka, E.; Cremer, D. *J. Phys. Chem. B* **2004**, *108*, 1115.

(26) Gräfenstein, J.; Cremer, D. *Chem. Phys. Lett.* **2004**, *387*, 415.

(27) Gräfenstein, J.; Cremer, D. *Chem. Phys. Lett.* **2004**, *383*, 332.

(28) Wu, A.; Cremer, D. *Phys. Chem. Chem. Phys.* **2003**, *5*, 4541.

(29) Gräfenstein, J.; Cremer, D., to be submitted for publication.

(30) Cremer, D.; Kraka, E.; Wu, A.; Lüttke, W. *ChemPhysChem* **2004**, *5*, 349.

(31) Gräfenstein, J.; Kraka, E.; Cremer, D. *J. Phys. Chem. A* **2004**, *108*, 4520.

(32) Gräfenstein, J.; Tuttle, T.; Cremer, D. *Phys. Chem. Chem. Phys.* **2005**, *7*, 452.

(33) Gräfenstein, J.; Cremer, D. *Magn. Reson. Chem.* **2004**, *42*, S138.

(34) Gräfenstein, J.; Cremer, D. *J. Chem. Phys.*, **2004**, *121*, 12217.

(35) (a) Åstrand, P. O.; Ruud, K.; Mikkelsen, K.; Helgaker, T., *J. Chem. Phys.* **1999**, *110*, 9463. (b) Ruden, A. T.; Lutnas, O. B.; Helgaker, T.; Ruud, K. *J. Chem. Phys.* **2003**, *118*, 9572.

(36) (a) Wu, A.; Cremer, D.; Auer, A. A. Gauss, J. *J. Phys. Chem. A* **2002**, *106*, 657. (b) Wu, A.; Cremer, D. *Int. J. Mol. Sci.* **2003**, *4*, 158.

(37) Wu, A.; Cremer, D. *J. Phys. Chem. A* **2003**, *107*, 1797.

(38) Zaccari, D.; Barone, V.; Peralta, J. E.; Contreras, R. H.; Taurian, O. E.; Diez, E.; Esteban, A. *Int. J. Mol. Sci.* **2003**, *4*, 93.

(39) Ruud, K.; Frediani, L.; Cammi, R.; Mennucci, B. *Int. J. Mol. Sci.* **2003**, *4*, 119.

(40) Lantto, P.; Vaara, J.; Helgaker, T. *J. Chem. Phys.* **2002**, *117*, 5998.

(41) Becke, A. D. *Phys. Rev. A* **1988**, *38*, 3098.

(42) Lee, C.; Yang, W.; Parr, R. P. *Phys. Rev. B* **1988**, *37*, 785.

(43) Dunning, T. H. Jr., *J. Chem. Phys.* **1989**, *90*, 1007.

(44) Boys, S. F. *Rev. Mod. Phys.* **1960**, *32*, 296.

(45) Huber, K. P.; Herzberg, G. *Constants of Diatomic Molecules*, Van Nostrand Reinhold: New York, 1979.

(46) Kraka. E.; Gräfenstein; J.; Filatov, M.; He, Y.; Gauss, J.; Wu, A.; Polo, V.; Olsson, L.; Konkoli, Z.; He. Z.; Cremer D. *COLOGNE 2004*; Göteborg University, Göteborg, Sweden, 2004.

(47) Berger, S.; Braun, S.; Kalinowski, H. O. *NMR-Spektroskopie von Nichtmetallen Band 4, ^{19}F-NMR-Spektroskopie*; Thieme: New York, 1994.

(48) Becke, A. D. *J. Chem. Phys.* **1993**, *98*, 5648.